
Particle streak velocimetry using Ensemble Convolutional Neural Networks

Alexander V. Grayver · Jerome Noir

Received: - / Accepted: -

Abstract This study reports an approach and presents its open-source implementation for quantitative analysis of experimental flows using streak images and Convolutional Neural Networks (CNN). The latter are applied to retrieve a length and an angle from streaks, which can be used to deduce kinetic energy and directionality (up to an 180° ambiguity) of an imaged flow. We developed a quick method for generating essentially unlimited number of training and validation images, which enabled efficient training. Additionally, we show how to apply an ensemble of CNNs to derive a formal uncertainty on the estimated quantities. The approach is validated on the numerical simulation of a convective turbulent flow and applied to a longitudinal libration flow experiment.

Keywords Streak analysis · Neural Networks · Turbulent Flows

1 Introduction

Particle Image Velocimetry (PIV) is arguably the most widely used technique to quantitatively study experimental flows [18, 14]. A common work-flow would consist of seeding a flow with luminescent particles and taking pairs of pictures with a known short time separation to capture an instantaneous flow state. By splitting a pair of images into (possibly overlapping) windows and cross-correlating between them allows one to infer the direction and magnitude of the flow. With

A. V. Grayver
Institute of Geophysics, ETH Zurich
Soneggstrasse 5
8092 Zurich, Switzerland
Tel.: +41-44-6333154
E-mail: agrayver@erdw.ethz.ch

J. Noir
Institute of Geophysics, ETH Zurich
Soneggstrasse 5
8092 Zurich, Switzerland
Tel.: +41-44-6337593
E-mail: jerome.noir@erdw.ethz.ch

modern computers and digital cameras, PIV has experienced wide adoption in the academic and industrial domains [17]. However, for cross-correlation to work properly, one has to ensure that the exposure time is short enough such that particles do not move more than a few pixels and the two images have clearly identifiable correlations [18]. Violating this condition, for instance because of an insufficient laser intensity or a too fast flow, results in so called streaks - traces of particles.

Streaks in the PIV images are commonly considered an experimental failure since they render cross-correlation techniques less efficient or even inapplicable. When flow velocity imposes constraints for which the camera and light source at hand cannot capture instantaneous particle positions, one either has to use a higher speed camera or/and a stronger light source. Both of these solutions quickly hit financial and safety constraints, which often cannot be overcome in academia. Therefore, there exists a need for alternative processing techniques. Although not suitable for conventional cross-correlation methods, streak images do carry information about the flow. Indeed, streaks provide quantitative information on the mean velocity magnitude and azimuth of the displacement of the particles over the exposure time of the frame. The only information lost in a streak image, when compared to a pair of PIV images, is the direction of the flow, leading to an ambiguity of 180° , no matter which algorithm will be used to analyze the images. Several methods can be used to extract quantitative information from a streak image. Among them is the probabilistic Hough transform [1], a widely used algorithm in computer vision to detect linear features in images. However, this approach requires fine tuning and often fails at coping with complex situations, such as overlapping streaks. To the best of authors knowledge, there are no other reliable algorithms to recover quantitative information from streaks images, which motivated us to design a new method using recent developments in the area of machine learning.

In particular, we applied an ensemble of Convolutional Neural Networks (CNN) trained on streak images to draw a statistical prediction of the displacement magnitude and corresponding azimuth. The potential of CNNs has long been recognized for applications related to the face and handwriting recognition [9, 15], although their power has been fully discovered only recently when deeper (that is, with more layers) networks became feasible to train within reasonable amount of time, mostly due to the emergence of affordable Graphic Processor Units (GPUs) [8, 7]. An interested reader is referred to a recent overview of the deep learning with important development milestones listed [10].

Before we proceed to describe methodology and results, it is worth to mention that a crucial ingredient to a success of CNNs is a suitably large training set, which a CNN is supposed to learn from without facing an over-fitting. From this perspective, building a training set from numerical simulations appears disadvantageous for two reasons: (i) producing a set of numerical simulations, which exhaustively cover the anticipated range of parameters is extremely resource demanding if not infeasible and (ii) since our main goal is to study fast turbulent flows, any numerical simulation will be band-limited, thereby lacking information on some wavelengths. In contrast, and similar to the PIV, we make a reasonable assumption that within a sufficiently small interrogation window velocity exhibits a simple functional form (for instance, constant or linear function). This allows us to quickly generate an unlimited number of window-based training images. Adding

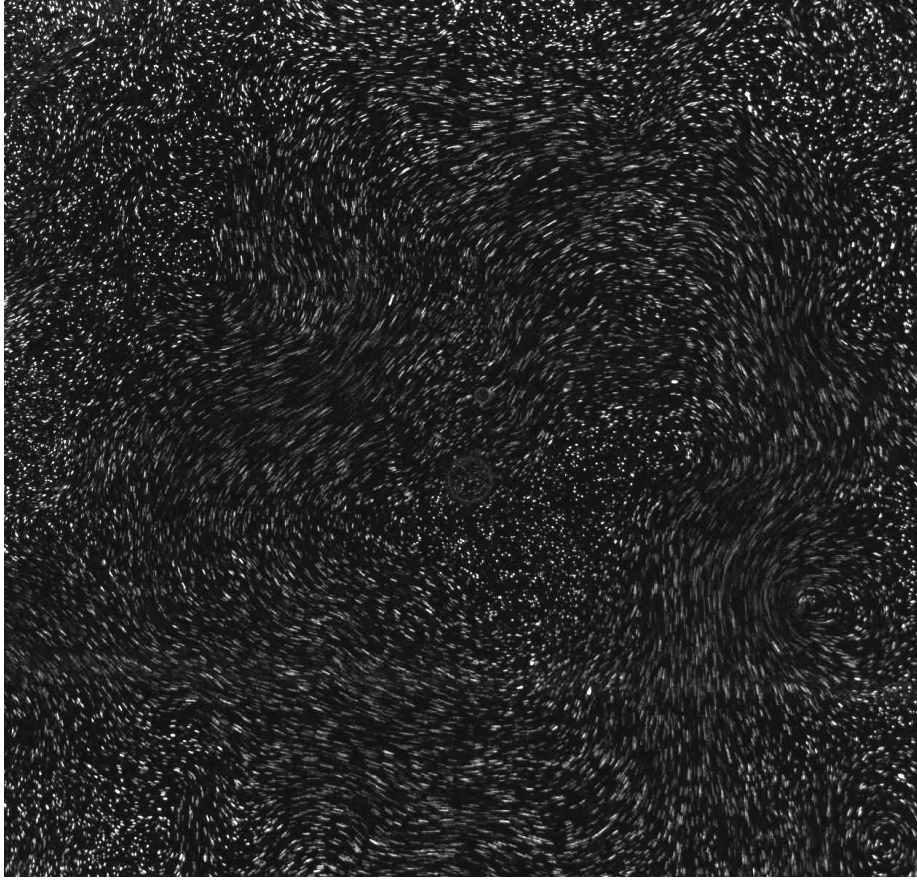


Fig. 1 Streaks image (1024×1024 pixels) from a longitudinal libration experiment in a cylindrical cavity. See section 3.3 for details

variability in number of streaks per window, their thickness and intensity mimics a realistic experimental scenario sufficiently well. Therefore, we can exhaustively sample the parameter space and feed the network with as many samples as needed to attain an acceptable accuracy. The specific numbers and parameters will be discussed in the corresponding sections below.

2 Methods

2.1 Problem setup

We aim at inferring the displacement and azimuth from a streak image of $N \times N$ pixels. A typical example is illustrated in Figure 1.

Similarly to how PIV is applied to a pair of images, we split an image into $(n \times n$, with $n = 48$ in this study) sub-windows with an overlap (50% in our case). Assuming the velocity is sufficiently uniform over the $(n \times n)$, we aim at

determining the mean length, that is the displacement over the exposure time, and azimuth for each sub-window.

A closer look at the image reveals that the number of streaks, their intensity and their width, vary within each sub-window. Additionally, in many cases, the streaks leave the $(n \times n)$ interrogation area. In order to make our CNN resilient to this variability, we generate train and validation images of $(48 \times 48$ pixels) with a random number of streaks varying between 2 and 10, a random color intensity between 90 and 255 and a random thickness between 2 and 4 pixels. The center of each streak is chosen randomly over the entire sub-window, such that streaks are allowed to go outside the image.

To generate train and validation images, we sampled displacement, Δ , and azimuth, ϕ , from uniform distributions

$$\Delta \sim U(1, \Delta_{\max}) \quad (1)$$

and

$$\phi \sim U(-\pi/2 + \delta, \pi/2), \quad (2)$$

respectively. Hence, in a single training or validation image all streaks have the same displacement and azimuth. Here, $\phi = 0$ corresponds to the positive x -axis and increases clockwise.

Note that limits for ϕ cover only half of the circle minus $\delta = 5^\circ$ on one end to mitigate ambiguity with respect to the direction. Once streaks are generated, the intensity within each streak is perturbed and the image is blurred with a Gaussian kernel of 3×3 pixels. In this study, the maximum displacement, Δ_{\max} , of a particle within an image is assumed to be half of the chosen window size, that is $r_{\max} = 24$ pixels.

Figure 2 shows a selection of streak images generated using the stated procedure. The outlined procedure enables generation of millions of images in just a few minutes on a regular PC.

2.2 Network architecture and implementation

We aim at building a regression CNN that, given a single window image, outputs two real numbers, corresponding to the displacement and azimuth. To this end, we have created a network with the architecture shown in Figure 3. As it can be seen, four convolutional units form the core of the network, each consisting of a convolutional layer, activation layer (in this case, rectified linear unit), average pooling layer used to downsample the input followed by a batch normalization layer. An increasing depth of the convolutional layers is a common choice aimed at giving a network ability to learn more complex features from the input. A fully connected (FC) layer at the end flattens the output of the convolution layers and, unlike previous layers, uses the trivial identity activation to transforms input parameters linearly into two output parameters, corresponding to predicted variables.

To prevent overfitting and improve training speed, we used batch normalization at the end of each convolution unit [6] and a dropout layer with the 30% drop fraction [16]. Additionally, following common practice, the outputs are standarized and centered. The input grayscale images have a single eight bits channel and are normalized by 255 to remain in the $[0, 1]$ range.

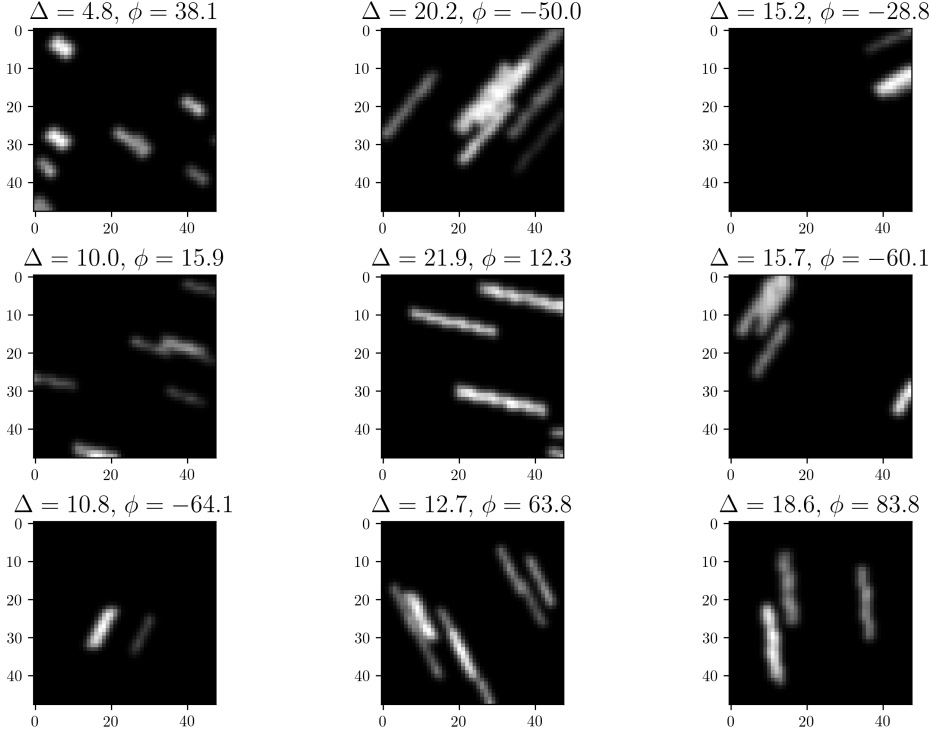


Fig. 2 Subset of generated streak images used for training and validation with the corresponding displacements (in pixels) and azimuth angles (in degrees) given in the titles.

Whereas there may exist more efficient architectures, we found that for our problem increasing the depth of the network did not improve the overall performance significantly, nor did increasing and/or decreasing filter sizes. Additionally, we found that, in contrast to majority of the reported CNN architectures, using the average pooling instead of the max pooling results in a slightly higher accuracy.

To increase accuracy and robustness of the prediction, we built an ensemble consisting of ten networks [4]. All networks have the same architecture and parameters, but were trained using different randomly chosen initial weights [2, 3] and random shuffling to form a unique sequence of batches supplied to an optimizer. The outputs of all ensemble members are averaged to obtain the final prediction and its variance. The latter serves as a proxy for the uncertainty of a prediction.

Finally, the network was implemented using the PyTorch library [12]. The complete implementation is open-source and can be found on the GitHub.

3 Results

3.1 Network training

We generated one million images (e.g., Figure 2) of which 75% and 25% were used for training and validation, respectively. Each network in the ensemble has been

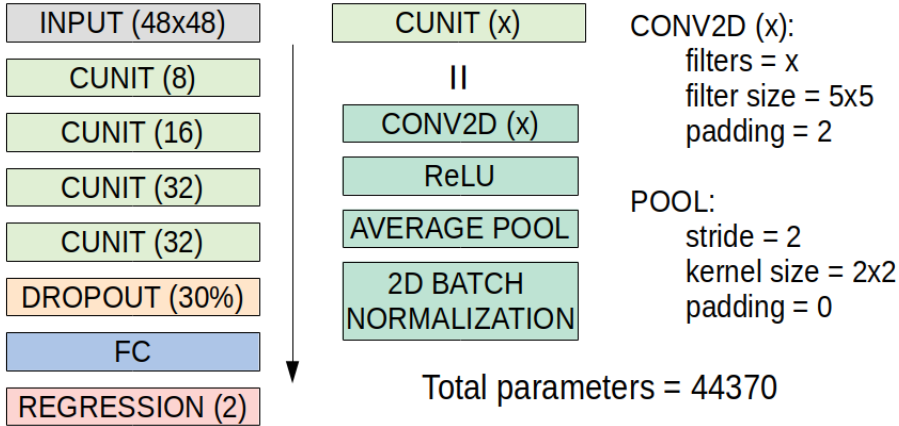


Fig. 3 Architecture of the used network. Left: sequence of layers and corresponding parameters in the brackets. Each CUNIT layer consists of four actual layers listed in the middle column. Relevant layer parameters are given on the right. Total number of learnable parameters in the network is 44370.

trained for 100 epochs. The ADAM optimizer with an initial learning rate value of 1e-3 was used. The learning rate was halved if no sufficient decrease in the validation loss was observed for the past 10 epochs. To make the training more robust to potential outliers (for instance, consider a situation when all streaks leave the window), we chose to minimize the Huber loss [5] rather than conventional least-squares loss. Huber loss represent a hybrid $L_2 - L_1$ distribution with a high tolerance to the presence of long tails in the original distribution. No pathologies between training and validation losses were observed during the training, specifically the validation loss remained a bit higher than the training loss, indicating that the network learns some generic features of the dataset. Training of each network took ≈ 90 minutes on a single CPU-GPU system. The modest training time makes it feasible to train networks for window sizes larger than the window of 48×48 pixels adopted here, although larger interrogation windows were not necessary for our problems.

Figure 4 shows RMSE values for all networks separately as well as the RMSE of the ensemble. RMSE was calculated as

$$\text{RMSE} = \sqrt{\frac{1}{N} \sum_{i=1}^N (x_i - \tilde{x}_i)^2}, \quad (3)$$

where \tilde{x} and x are the true and predicted values of Δ or ϕ , respectively.

It is evident that the ensemble performs systematically better than any single network. CNN ensemble achieves the accuracy of 1.05 pixels for the displacement and 8.5° for the angle predictions, respectively. The latter may seem like a large error, however one should realize that having a 48×48 pixels window inevitably leads to limitations in recognizing small rotations, especially when streaks are short.

Figure 5 shows a random selection of validation images with the corresponding ensemble CNN predictions and true values. We see that the ensemble CNN

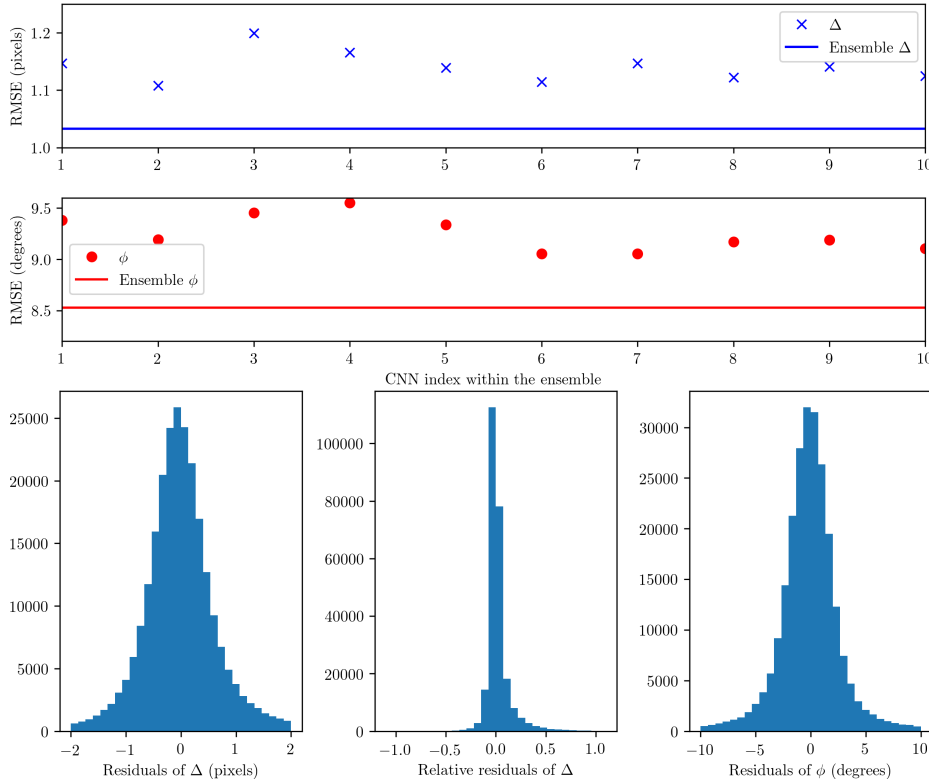


Fig. 4 Top: RMSE values of individual networks (markers) and ensemble (line) for displacement Δ and angle ϕ calculated on the validation set. Bottom: histograms of the residuals for the displacement and angle. Histograms for both absolute and relative (i.e., normalized by the true displacement) residuals are shown.

has learned to make accurate prediction even for complex situations when some streaks overlap, join or leave the window. For instance, in Figure 5(bottom row, middle), two streaks coincidentally joined and formed what appears to be a longer streak, but CNN prediction is not confused since other streaks provide enough information for an accurate prediction. Additionally, Figure 6 shows nine images which produced the worst predictions of the displacement. Clearly, most of these cases are associated with situations where originally longer streaks have all been displaced outside the window. Note that such situations do not represent a failure of the CNN, but rather limitation of the window-based approach. Similar situations are likely to occur in experimental images and unfortunately they leave little chance for any sliding window approach to make an accurate prediction. We will discuss possible ways to mitigate this in the Conclusions section. It is worth to note that despite an inaccurate displacement prediction, the angle is predicted accurately in most of these cases.

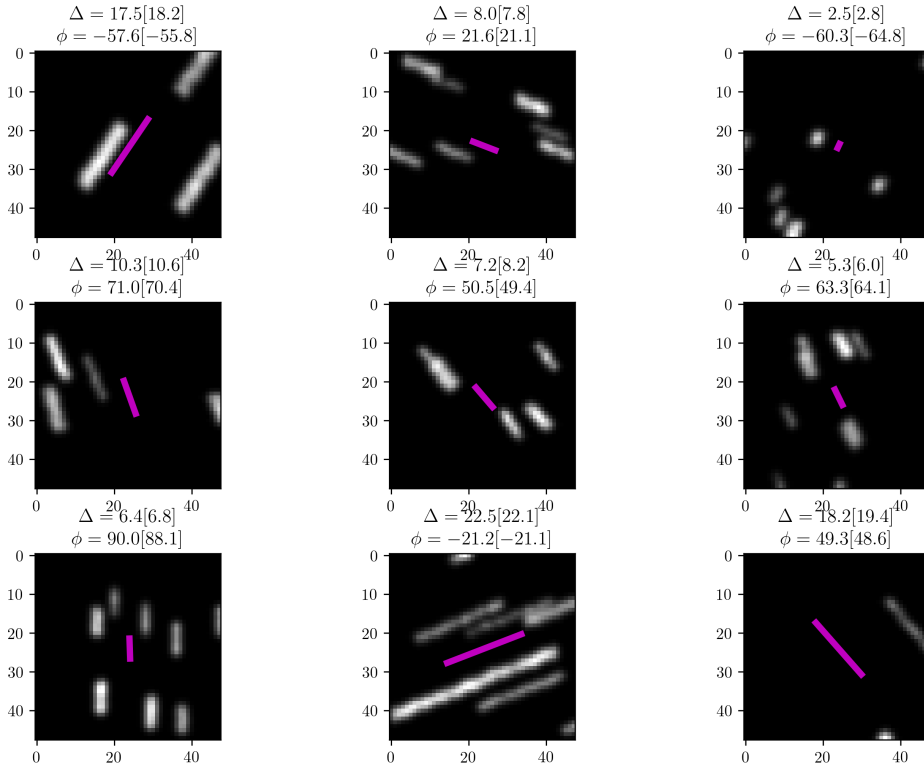


Fig. 5 Random images with the predicted displacement and angle depicted as magenta lines. The true values are given in titles and predicted values in brackets.

3.2 Validation using synthetic flows from numerical simulations.

After confirming the excellent performance of the network on the validation set, we turn to a direct numerical simulation (3D-DNS) of a complex thermal convection turbulent flow published recently [13]. In their paper, the authors simulate rapidly rotating thermal convection in a square box, heated from below and cooled from the top with a vertical gravitational field pointing downward and a vertical axis of rotation. To validate our CNN algorithm, we used a simulation obtained for $E = 10^{-7}$, where E is the Ekman number representing the ratio of viscous to rotational effects, and a Raleigh number that is 90 times the supercritical. Each velocity field is calculated on a uniform grid of size 192^3 . For the purpose of this study, we extracted the horizontal component of the velocity in a horizontal plane at mid-depth. Because of the limited resolution of the simulation, each velocity component has been interpolate on a 1024×1024 pixels grid. Figure 7 left shows the displacement map obtained from the full DNS for an arbitrary exposure time. Since the CNN will act on (48×48) interrogation windows with the 50% overlap, we apply a sliding window averaging with (48×48) and 50% overlap (Figure 7, right). The window averaged displacement is the best reconstruction we can possibly achieve with a 48×48 pixels window and a 50% overlap used in this study, thus all later results will be compared against it.

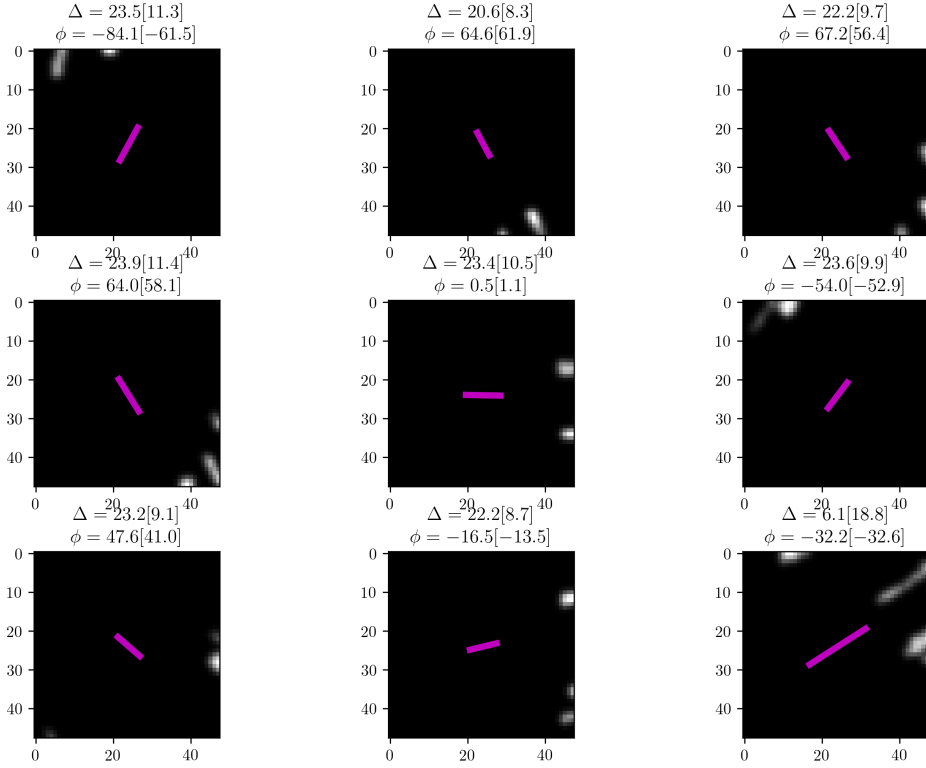


Fig. 6 Same as previous, but showing nine worst prediction in terms of displacement.

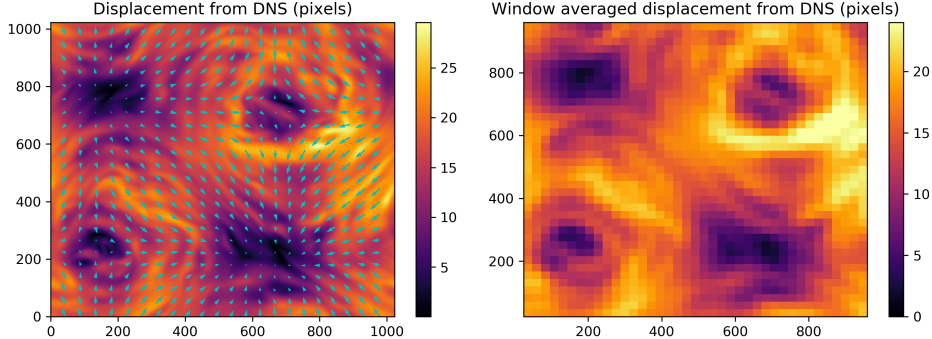


Fig. 7 Original (left) and window averaged (right) displacement maps of the DNS [13] used for validation. The arrows on the left show the true horizontal vector field from the DNS.

To reduce subjectivity, we generated 30 randomly seeded streak images using the original DNS velocity (Figure 7, left). We first split the image into 48×48 pixels subwindows, inside which we calculate the mean linear displacement $\mathbf{d} = \bar{\mathbf{u}}dt$, where $\bar{\mathbf{u}}$ represents the horizontal velocity average over 48×48 pixels. In each subwindow we generate a random seeding, varying the density (from 1 to 10 seeds per subwindow) and radius (from 2 to 4 pixels) of the seeds and reconstruct the associated streaks. Finally we apply a Gaussian filter with a kernel of 3×3 pixels

to mimic the natural variability of intensity observed in experimental images. We repeat the entire process to generate 30 independent streak images from the same velocity field. The trained CNN ensemble was applied to all images and the resulting averaged reconstruction of both displacement and angle are shown in Figure 8. We see that the reconstructed images recover the general structure of the flow very well. The only undesired effect is that the ensemble CNN struggles to correctly predict large displacements. When the displacement reaches half of the window size, CNN systematically predicts smaller displacements. The reason for this is not a deficiency of the CNN, but rather the fact that for displacements as large as half the window size it becomes very likely that most of the streaks go outside the window, thus a smaller displacement is a rational prediction. To solve this problem, one could apply a larger window (for instance, 64×64 pixels), although this will reduce the overall resolution and may render constant velocity assumption less accurate. In real experimental settings, it may be advantageous to apply several window sizes and either choose one or combine obtained results, depending on a particular experimental setup.

Additionally, we compared the performance of the CNN ensemble with a more conventional technique based on the probabilistic Hough transform [1]. The results of the Hough transform are shown in Figure 8. Clearly, approach based on the Hough transform shows a less robust behaviour, especially in predicting the displacement.

Finally, Figure 9 shows one of the streak images generated from the DNS with the true and predicted streaks for each window position. Note that while the whole velocity field is used to generate the background streak images, the overlying red streaks are reconstructed at the location of the CNN grid point using the averaged displacement and angle maps (Figure 7). Generally, the ensemble CNN performs well. There is, however, accuracy reduction in regions of large displacements for reasons described above and across areas of vertical shearing, where angle predictions become locally less accurate. Interestingly, these vertical shear regions also lead to abnormal streaks orientation (close to horizontal) when using the window averaged field values of the DNS itself (red streaks in Figure 9).

3.3 Application to the flow driven by longitudinal libration in laboratory experiment

Finally, we apply our algorithm to a laboratory experiment depicted in Figure 10. The apparatus consists of a straight cylinder filled with water and set in rotation on a turntable at 1Hz. The cavity is 286 mm high with a radius of 140 mm. The bottom lead is covered with a topography made of blocks ($64 \times 64 \times 8$ mm). A second motor is used to oscillate the container on the turntable, resulting in the so-called longitudinal libration.

In such a system, flows at low libration amplitudes are in the form of linear inertial waves and inertial modes. As the amplitude increases, the flows become unstable and eventually saturate with a significant geostrophic component, i.e. mainly two dimensional. For the purpose of this experimental validation, we have set the libration frequency to 1Hz and the amplitude to 34° , which corresponds to the geostrophic saturation state aforementioned.

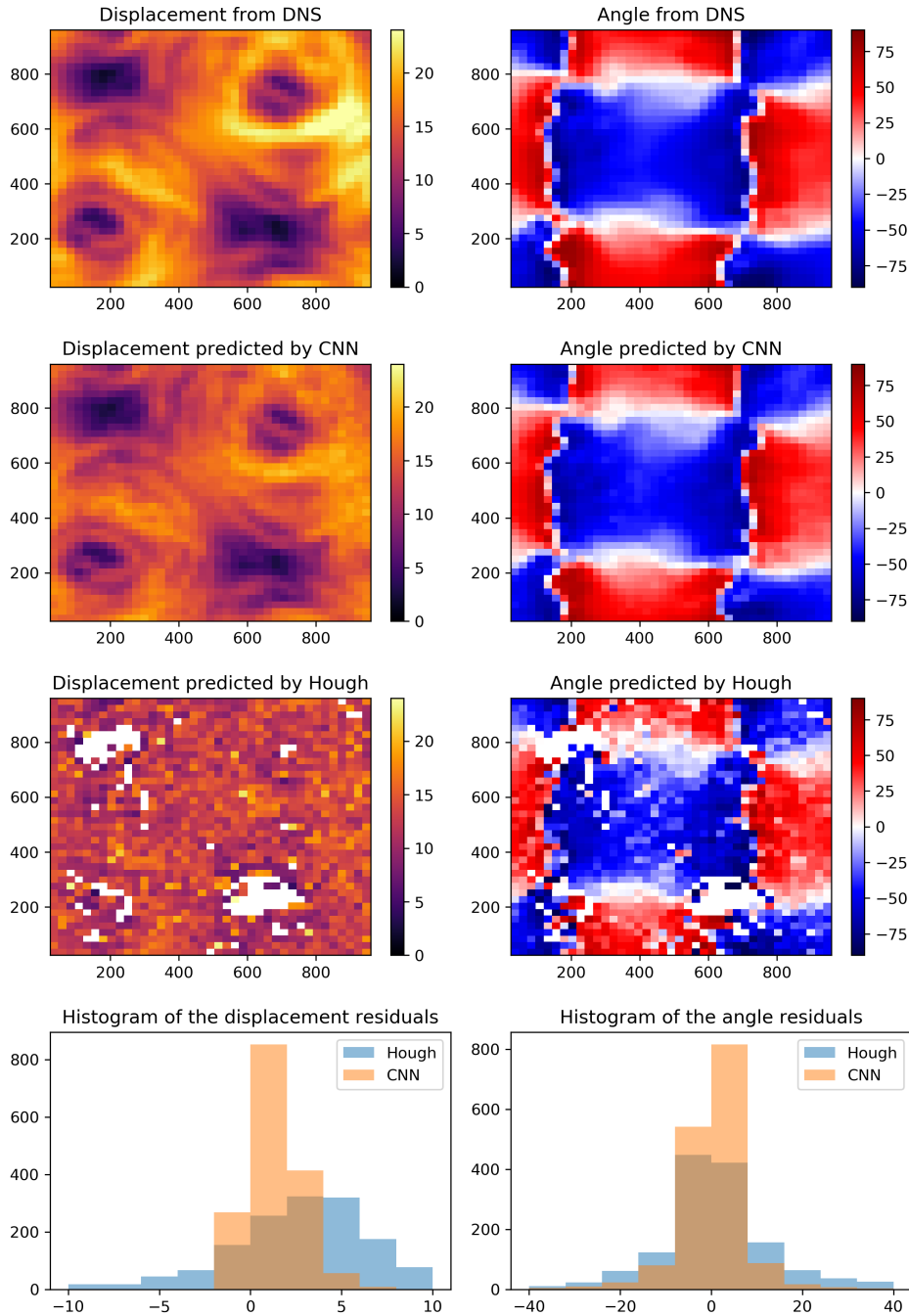


Fig. 8 Original displacement and angle (top row) along with the predicted values obtained by using proposed ensemble CNN and more conventional Hough transform methods (see text for more details). Bottom: histograms of the residuals between true and predicted values for both methods.

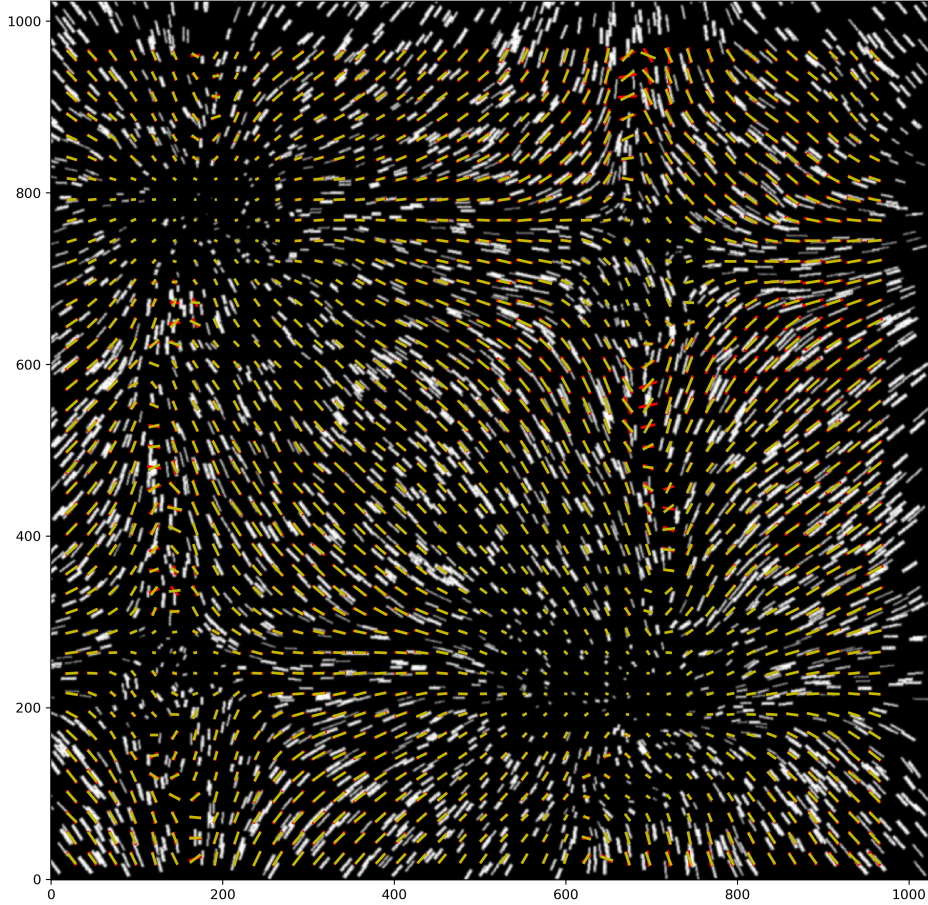


Fig. 9 Streak image generated from the DNS with true and predicted displacement and angle shown as red and yellow lines, respectively.

To image the flow, we use a one Watt continuous diode laser to illuminate a horizontal plane of the fluid seeded with fluorescent particles. The particles absorb in the green and emit in the orange. By mounting a narrow band pass filter on the lens of the camera, we reject the light coming from the reflections of the laser on the side walls. While greatly improving the contrast of the images, the use of a band pass filter reduces the amount of light reaching the CCD sensor, as a consequence we must work with relatively large exposure time of 21ms with a sampling frequency of 30 images per second. This limitation leads to streak images as shown in Figure 1 rather than sharp images of individual particles that would be appropriate for PIV. Meanwhile, our CNN algorithm is well suited for extracting quantitative information from this type of images. We first apply our algorithm to a single frame prior to analysing image sequence covering 10s of the libration in a statistically steady state.

A pre-processing step was necessary for real images to filter out the CCD matrix noise. We achieved this by a simple thresholding of the image intensity at

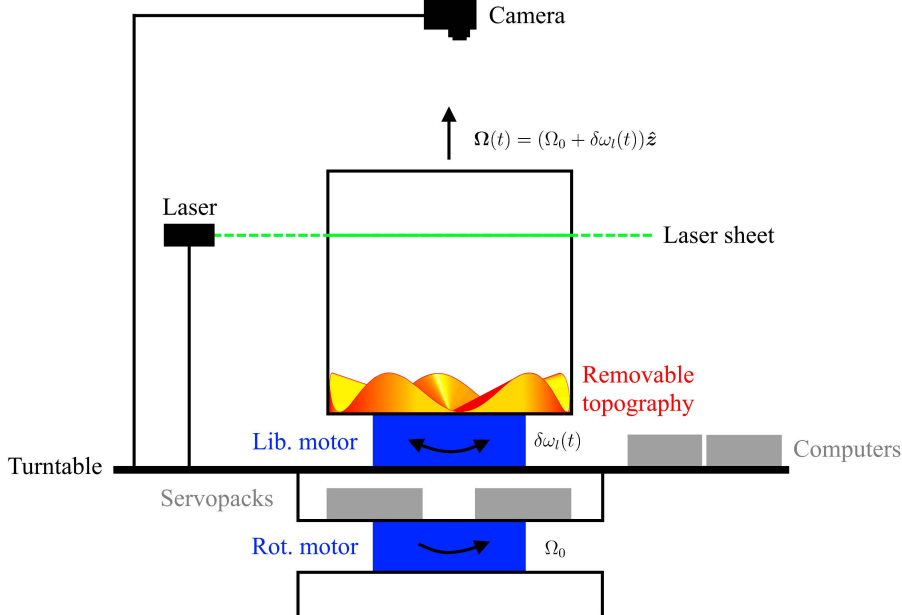


Fig. 10 Experimental setup of the longitudinal libration experiment [11].

the value of 50. After that, image was split into overlapping 48×48 pixels windows, resulting in a total of 2400 window images. The ensemble CNN was then applied to predict displacements and angles as well as their standard deviations with the latter serving to be a proxy for the output uncertainties.

Figures 11-12 show the predictions of the displacement and azimuth in the form of maps and histograms for one randomly chosen frame of the movie. Figure 13 shows the selected experimental image we used and window-centered predictions drawn as lines. First of all, we see that experimental flow exhibits rather complex structure, with regions where streaks show non-linear behaviour of the flow within a window, which violates our initial assumptions. Nonetheless, the ensemble CNN produces coherent and spatially correlated predictions (Figure 11). It is also interesting to analyse the standard deviation maps (Figure 12). Large absolute errors in the displacement map appear to be correlated with regions of fast flow. On the other hand, large uncertainties in the angle occur around regions with vertical velocity shear, as observed in DNS synthetic images, specifically where velocity seems to flip the direction.

After checking that the algorithm behaves well on a single frame, we applied the CNN ensemble to 300 frames taken at 30 fps to capture the temporal evolution of the flow. Subsequently, we calculated the mean kinetic energy from the displacement for each frame as

$$E = \frac{1}{P} \sum_{i=1}^P \left(\Delta_i \frac{l}{\tau} \right)^2, \quad (4)$$

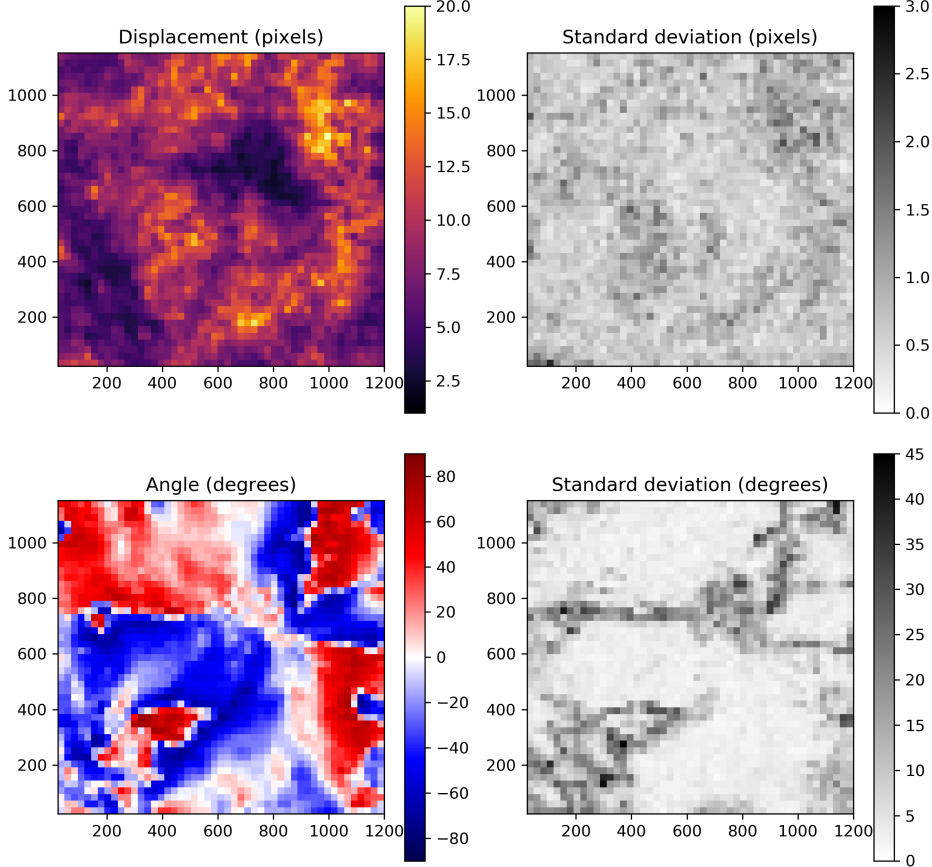


Fig. 11 Predicted displacement and angle (left) along with their standard deviations (right) inferred from the ensemble CNN for an experimental image shown in Figure 13.

where P is the number of grid points in a frame, Δ_i is the i -th displacement in pixels, $l = 0.25 \cdot 10^{-3}$ m/pixel is the calibration factor from pixels to meters for our optical setup, $\tau = 21$ ms the exposure time. The timer-series of the mean kinetic energy and its Power Spectral Density are shown in Figure 14. As anticipated, we can clearly identify the dominant forcing frequency of 1 Hz and the harmonics at 2 Hz and 3 Hz, resulting from non-linear effects.

In terms of performance, ensemble CNN attains a speed of seven full images (each totaling to 2400 windows) per second on an NVIDIA GoForce GTX 1070Ti powered PC. This level of performance allows us to comfortably process long sequences of images taken during experiment, which we use to study evolution of the kinetic energy. Using a more modern GPU will likely also enable real-time predictions at rates of a few dozens of images per second, which could be more relevant for industrial applications.

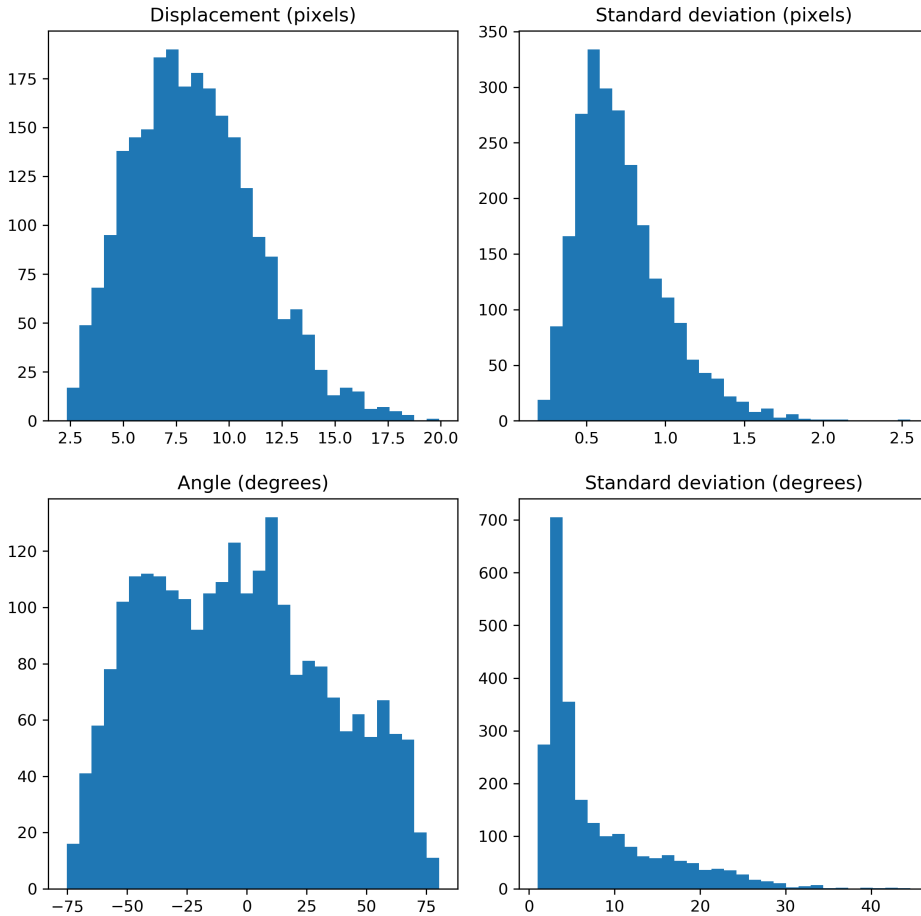


Fig. 12 Same as above, but in a form of histograms.

4 Conclusions

We presented an open-source ensemble CNN aimed at quantitative analysis of complex experimental flows using streak images. The presented approach can be applied in situations when classical PIV is inaccurate or not possible due to experimental setup or hardware limitations. The advantage of the presented approach is the ease of training/validation set generation as well as recovery of the prediction uncertainty through application of the ensemble method. We foresee that the approach may need an experiment-dependent tailoring to achieve the best performance. According to our experience, this only takes a single day on an average PC equipped with a modern GPU.

The potential extensions of the presented approach may include the use of multiple window sizes applied to the same image, more complex functional parameterizations of the displacement and angle fields within a window (e.g., using a polynomial). Finally, a completely different approach based on an image segmentation and object localization and/or tracking can be applied to extract information

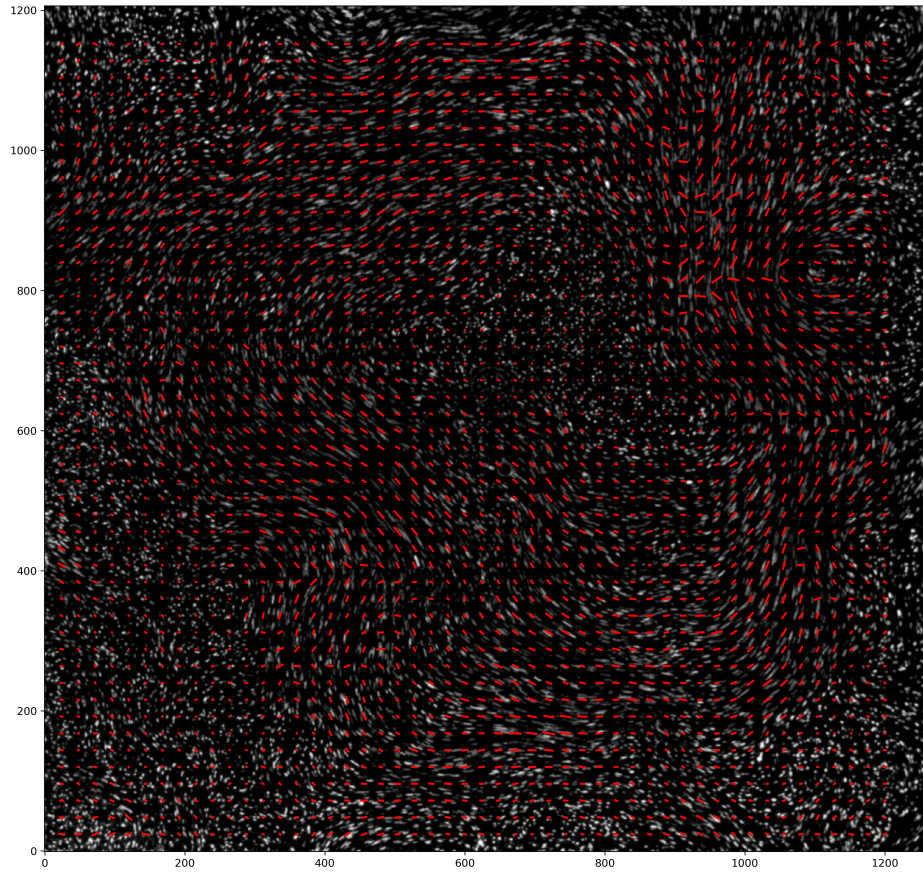


Fig. 13 Streak image taken during an experiment overlain by the predicted displacement and angle shown as red lines.

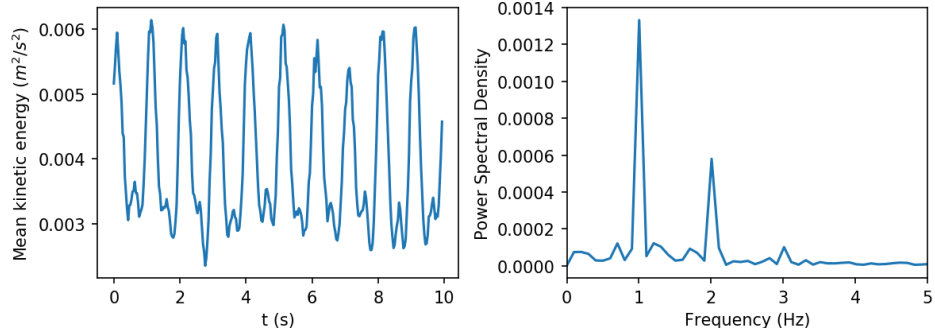


Fig. 14 Left: Mean flow kinetic energy calculated from the displacement in each frame of the movie. Right: Normalized power spectral density of the mean kinetic energy.

about individual streaks and their evolution in time. We hope to investigate these directions in details in our future studies.

Acknowledgements We thank authors of PyTorch, matplotlib and h5py libraries for making them available, Meredith Plumley for sharing her DNS data, Adrian Tasistro-Hart for a number of insightful discussions on CNNs. Comments by two anonymous reviewers helped improve the manuscript. The Jupyter Python notebooks of all programs used in this study can be found here <https://github.com/agrayver/streakcnn>.

References

1. Galamhos, C., Matas, J. and Kittler, J.: Progressive probabilistic Hough transform for line detection. Proceedings. IEEE Computer Society Conference on Computer Vision and Pattern Recognition, pp. 554–560 (1999)
2. Glorot, X., Bengio, Y.: Understanding the difficulty of training deep feedforward neural networks. In: Proceedings of the thirteenth international conference on artificial intelligence and statistics, pp. 249–256 (2010)
3. He, K., Zhang, X., Ren, S., Sun, J.: Delving deep into rectifiers: Surpassing human-level performance on imagenet classification. In: Proceedings of the IEEE international conference on computer vision, pp. 1026–1034 (2015)
4. Hinton, G., Vinyals, O., Dean, J.: Distilling the knowledge in a neural network. arXiv preprint arXiv:1503.02531 (2015)
5. Huber, P.J., et al.: Robust regression: asymptotics, conjectures and monte carlo. *The Annals of Statistics* **1**(5), 799–821 (1973)
6. Ioffe, S., Szegedy, C.: Batch normalization: Accelerating deep network training by reducing internal covariate shift. arXiv preprint arXiv:1502.03167 (2015)
7. Karpathy, A., Toderici, G., Shetty, S., Leung, T., Sukthankar, R., Fei-Fei, L.: Large-scale video classification with convolutional neural networks. In: Proceedings of the IEEE conference on Computer Vision and Pattern Recognition, pp. 1725–1732 (2014)
8. Krizhevsky, A., Sutskever, I., Hinton, G.E.: Imagenet classification with deep convolutional neural networks. In: Advances in neural information processing systems, pp. 1097–1105 (2012)
9. Lawrence, S., Giles, C.L., Tsoi, A.C., Back, A.D.: Face recognition: A convolutional neural-network approach. *IEEE transactions on neural networks* **8**(1), 98–113 (1997)
10. LeCun, Y., Bengio, Y., Hinton, G.: Deep learning. *nature* **521**(7553), 436 (2015)
11. Meister, A.: Effects of boundary topography on the flow forced by libration in longitude in a rotating cylinder, master thesis, ETH Zurich, (2018)
12. Paszke, A., Gross, S., Chintala, S., Chanan, G., Yang, E., DeVito, Z., Lin, Z., Desmaison, A., Antiga, L., Lerer, A.: Automatic differentiation in PyTorch. In: NIPS-W (2017)
13. Plumley, M., Julien, K., Marti, P., Stellmach, S.: The effects of Ekman pumping on quasi-geostrophic Rayleigh–Bénard convection. *Journal of Fluid Mechanics* **803**, 51–71 (2016)
14. Raffel, M., Willert, C.E., Scarano, F., Kähler, C.J., Wereley, S.T., Kompenhans, J.: Particle image velocimetry: a practical guide. Springer (2018)

15. Simard, P.Y., Steinkraus, D., Platt, J.C., et al.: Best practices for convolutional neural networks applied to visual document analysis. In: Icdar, vol. 3 (2003)
16. Srivastava, N., Hinton, G., Krizhevsky, A., Sutskever, I., Salakhutdinov, R.: Dropout: a simple way to prevent neural networks from overfitting. *The Journal of Machine Learning Research* **15**(1), 1929–1958 (2014)
17. Tropea, C., Yarin, A.L.: Springer handbook of experimental fluid mechanics. Springer Science & Business Media (2007)
18. Westerweel, J.: Fundamentals of digital particle image velocimetry. *Measurement science and technology* **8**(12), 1379 (1997)